Contrib Mineral Petrol (2004) 146: 671–682
DOI 10.1007/s00410-003-0522-6

ORIGINAL PAPER

Oliver Schenk · Janos L. Urai

Microstructural evolution and grain boundary structure during static recrystallization in synthetic polycrystals of Sodium Chloride containing saturated brine

Received: 11 February 2003 / Accepted: 23 September 2003 / Published online: 11 November 2003

Abstract The effects of brine on recrystallization in halite are well known. However, properties of brine such as morphology, connectivity, diffusivity and the resulting influences on deformation mechanisms are still a matter of debate. This paper presents a microstructural study of dense, statically recrystallizing synthetic polycrystalline halite containing small amounts of brine. We used powders of two different grain size classes: < 10 μm and 200–355 μm. The aggregates were compacted to brine-filled porosities less than about 2% and annealed at room temperature, without an external stress field.

Coarse-grained samples undergo *recrystallization* manifested by the growth of large (up to 300 μm) strain-free grains into the deformed old grains. The new grains are frequently euhedral, with mobile grain boundaries moving at rates up to 6 nm/s. Their mobility is interpreted to be high due to the presence of water. Grain surfaces are smooth and the width of the water-rich zones is usually below the resolution of the SEM (less than 50 nm).

The evolution of fine-grained samples starts with primary recrystallization and a reorganization of grain boundaries. After this stage, which lasts a few hours, *normal grain growth* effectively stops, and no significant increase of grain size is observed even after several months. Microstructural observations indicate contact healing at the grain boundaries, with dihedral angles ranging between 20 and 110°. We interpret these boundaries to be fluid-free, with the brine residing in a network of triple junction tubes. This system of triple junctions is interconnected and associated with significant permeability.

While grain growth is inhibited in the fine-grained samples, after a few hours of annealing *exaggerated grain growth* is commonly initiated. This is manifested by the growth of large, euhedral grains replacing the fine-grained matrix. These grains also grow with low-index facets and their boundaries are also interpreted to be mobile due to the existence of a water-rich phase.

Editorial Responsibility: J. Hoefs

O. Schenk (✉) · J. L. Urai
Geologie - Endogene Dynamik, RWTH Aachen,
52056 Aachen, Germany
E-mail: o.schenk@ged.rwth-aachen.de
Tel.: +49-241-8095416
Fax: +49-241-8092358

Introduction

The presence of brine in halite strongly affects its mechanical and transport properties. Observations from nature and experiments show that in deforming wet halite solution transfer creep and dynamic recrystallization are dramatically enhanced, and that fluid distribution is complex, both during and after deformation. Understanding the fluid distribution is important for modeling and prediction of processes in a wide range of geological environments, such as the seasonal movement of salt glaciers (Wenkert 1979; Talbot and Rogers 1980), strain localization in shear zones in salt (Miralles et al. 2001), and the flow of salt during diapiric movement (Jackson and Talbot 1986). There is also interest in applied fields, e.g. to predict the behavior of underground caverns (Fokker et al. 1996) or modeling properties of salt as seals for gas or oil (Lewis and Holness 1996; Holness and Lewis 1997; Peach et al. 2001).

The reason for the complexity in brine distribution is the high solubility and diffusivity of sodium chloride in water, even at room temperature. Therefore, in addition to the redistribution of the fluid under stress by viscous flow (with high viscosities in very thin fluid films (Peach et al. 2001)) during grain boundary sliding and microcracking, this high solubility and diffusivity may lead to solution and crystallization processes in grain boundaries, driven by local gradients in chemical potential, due to the presence of external stress, dislocations, grain boundaries, solid solution impurities or other defects.

Two end members of this grain boundary process are pressure solution (Spiers et al. 1990) and fluid-assisted grain boundary migration (Urai et al. 1986b; Watanabe and Peach 2002). Although these two end members are quite different, the process of dissolution and precipitation is common to both, and several transitional processes can be envisaged (Urai et al. 1986a). This is further illustrated in Fig. 1. Here we consider two crystals A and B, with two marker points a and b, respectively, separated by a boundary. We describe this bicrystal in a coordinate system of which the origin is fixed at the boundary, the y-axis is along the boundary and the x-axis is at 90° to the boundary. We then define V_a and V_b as the x-components of velocity of the two marker points a and b on both crystals. We now plot V_a vs V_b. For the case of a migrating, conservative grain boundary, the velocities will plot on the line $V_a = V_b$, i.e. both crystals move to the right or left at equal velocity. For pressure solution, the velocities will plot in the top left quadrant: on the line $V_a = -V_b$ both crystals will dissolve at equal rates. The diagonal in the bottom right quadrant represents a crack-seal accretion process where the two crystals both move apart and grow at the same rate (Hilgers et al. 2001; Hilgers and Urai 2002).

The off-diagonal positions represent general grain boundaries at which dissolution or accretion rates are unequal on both sides. For the case of grain boundary migration this means that the motion is non-conservative (involving addition or removal of material). For the case of pressure solution this means that material on both sides is not removed at equal rates.

Urai et al. (1986a) proposed briefly the possibility of such general boundaries. Their importance has become clearer based on the work of de Bresser et al. (2001), who argued that dynamic recrystallization brings a polycrystal to the transition region between grain size sensitive and grain size insensitive creep fields, so that grain boundary migration, dissolution and precipitation processes occur quite naturally together, all at significant rates. In such a material general grain boundaries should be the rule rather than exception.

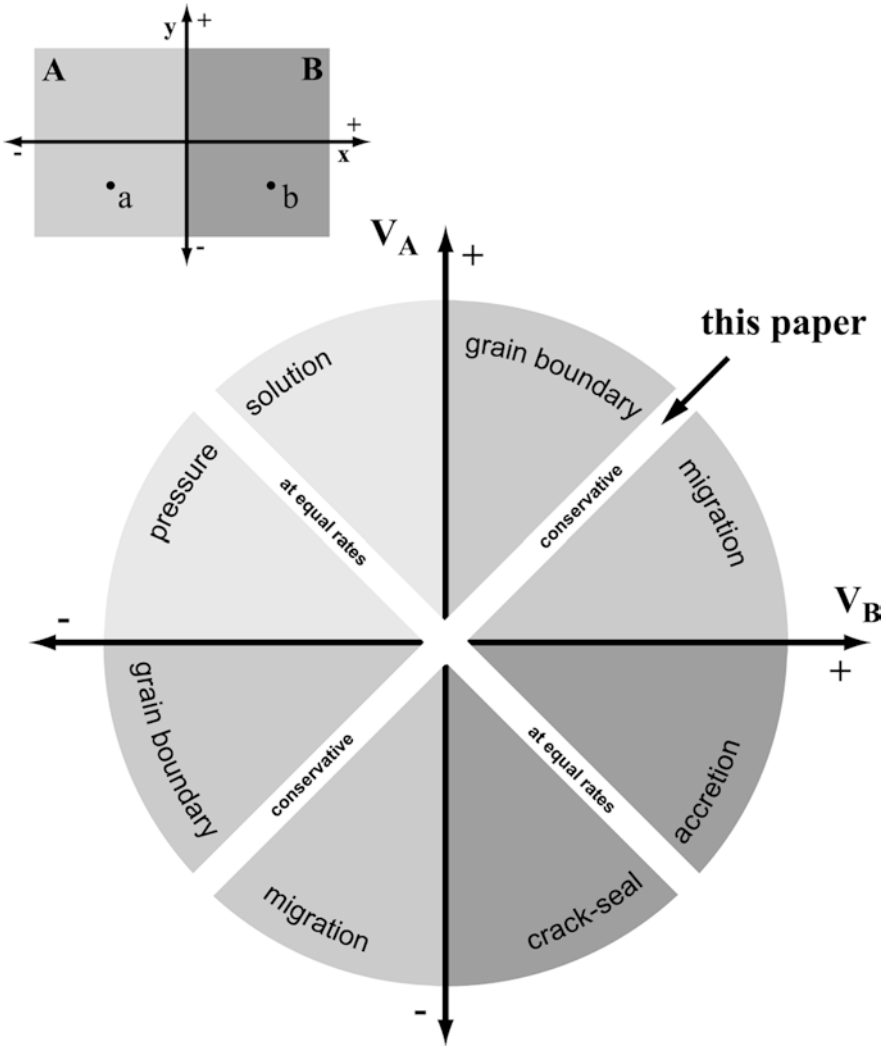

Fig. 1 Schematic diagram illustrating the relationship between different processes in general, non-conservative grain boundaries. See text for detailed description

The large effect of water on the recrystallization process in sodium chloride is well documented. Skrotzki and Welch (1983), Urai et al. (1986a, b), Drury and Urai (1990), Spiers et al. (1990), Peach et al. (2001), and Watanabe and Peach (2002), have shown that between room temperature and 150 °C wet, polycrystalline, natural samples deformed in the non-dilatant field recrystallize readily during and after deformation, and have presented observations which can be interpreted as that the boundaries contain thin brine films. In comparison, the experiments of Guillopé and Poirier (1979) and Franssen (1993), with dry sodium chloride showed that grain boundaries are essentially immobile at temperatures below 400 °C. A model for the migration of water-containing boundaries, based on the serial processes of dissolution, diffusion through the fluid and crystallization was proposed by Urai et al. (1986a) and Garcia Celma et al. (1988). This model was further expanded by Peach et al. (2001) and Watanabe and Peach (2002), who also included interface reaction control of the migration rate into their calculations.

One of the criticisms of the model of fluid films on mobile grain boundaries was based on the fact that the samples, which recrystallized in an anisotropic stress state, were examined after removal of the stress. This could have led to a redistribution of the fluid by viscous flow, possibly to evaporation of the fluid, and thus to errors of interpretation.

Another argument is based on consideration of thermodynamic equilibrium, where at room temperature and a pressure of 1 bar the contact angle between sodium chloride and brine is about 70°. This should lead to contact healing (Smith 1964; Lewis and Holness 1996; Holness and Lewis 1997). If fluid films exist at some stage, it is not clear how and how long they can be maintained in such a system.

Pressure solution experiments on wet halite (Spiers et al. 1990; Spiers and Schutjens 1990; Peach 1991; Schutjens 1991; Hickman and Evans 1991; Martin et al. 1999; de Meer et al. 2002) have shown that this process is dramatically enhanced by the presence of brine, and that the grain boundaries often have an island-channel structure at length scales of micrometers. This is quite different to the structures observed in mobile grain boundaries, where the grain surfaces are smooth (Urai et al. 1986b). Transitional behavior may have played a role in the experiments of Spiers and Brzesowsky (1993), who found recrystallization in compaction experiments dominated by pressure solution at pressures larger than 4 MPa.

Under suitable conditions, contact healing was also shown to occur in pressure solution experiments (Hickman and Evans 1991; Visser 1999). The theoretical basis of grain contact healing under stress was further presented by Visser (1999), who considered surface energy terms in addition to stress-related driving forces and predicted the fields for pressure solution, contact healing and neck growth.

Aims of this study

The aim of this study was to better understand the effect of small amounts of brine on the migration of grain boundaries in halite, and to obtain constraints on the properties of the brine in these grain boundaries.

To avoid redistribution of the fluid by viscous flow after removal of stress, samples were annealed under atmospheric pressure, without deformation.

Methods

Wet synthetic polycrystalline halite samples were cold-pressed from powders of analytical grade NaCl (Roth, Art. 9265.3; NaCl content $>99.9\%$) or table salt. We compacted wet sodium chloride powder of two different grain size classes (<10 μm and 200–355 μm) to dense aggregates with brine-filled porosities less than 2% which were annealed at room temperature. The microstructural evolution was studied by scanning electron- and reflected light microscopy of surfaces that were either polished and etched or broken.

Preparation of powders

Two sets of samples were prepared, differing only in the grain size of the starting material:

1. Coarse-grained starting material: the grain size of 200–355 μm was obtained by sieving the as-received NaCl powder.
2. Fine-grained starting material: dry NaCl powder was ground in a swingmill. Remaining coarse grains were extracted by Stokes separation: after grinding again in a saturated NaCl solution in an agate mortar, the slurry was poured into a column containing saturated NaCl solution, and decanted after the coarse grains settled on the bottom. The main problem with this method was that the grains in the powder tended to cluster, preventing full dispersion of the fine-grained fraction. This procedure was repeated for a second time to produce grains of dominantly 5–10 μm containing rare larger grains of about 15 μm, suspended in the saturated solution.

Compaction

After treating for 30 seconds in an ultrasonic bath, the salt brine mixture was poured into a cylindrical die (Fig. 2). An O-ring on the lower piston sealed the vessel from below, while the weight of the upper piston (without O-ring) allowed most of the brine to slowly drain out on the top. Subsequently the pressure on the upper piston was raised to 150 MPa in a few minutes, and maintained for 5 minutes. Then the pressure was removed, and the sample was extracted from the die by removing the upper piston and pressing the lower piston upwards. The unconsolidated material in the die had a height of 6–8 mm, producing dense cylindrical samples with a diameter of 1 cm and a height of 2–4 mm. This aspect ratio was chosen to avoid density differences in the sample due to friction along the die's wall during pressing.

The samples produced had $97.5 \pm 0.5\%$ theoretical density, containing a small amount of saturated brine as a pore fluid. The procedure was developed to minimize the possibility of introduction of gas bubbles in the samples, so that the pores were brine-filled.

For comparison, an equivalent set of samples was prepared, with cyclohexane as pore fluid of a dried (104 °C for 3 days) coarse-grained powder.

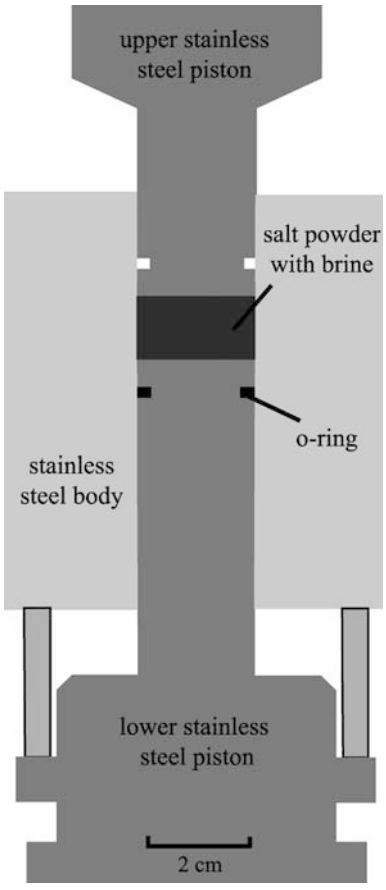

Fig. 2 Schematic diagram of the uniaxial compaction apparatus

Annealing

To study the evolution of the microstructure in combination with the influence of fluids, the brine-filled samples were annealed in small, air-tight containers containing a small amount of saturated NaCl solution, not in contact with the samples. This ensured that the vapor pressure of H_2O around the sample was buffered at the equilibrium value. The annealing was carried out at room temperature and at 80 °C, in this paper we report the results of the experiments at a temperature of 24 ± 1 °C.

Sample preparation for microscopy

The samples, which recrystallize at room temperature, cannot be quenched. When a sample's outer surface has been prepared for microscopy, the sample may continue recrystallizing and modifying its structure. This possibility was carefully evaluated by observing the same surface as a function of time, until we were convinced that the outer surface of the samples does not change with time.

Many samples showed some efflorescence after removal from the annealing cell, pointing to a network of connected, fluid-filled pores in the sample.

Polished and etched surfaces

The observation of grain boundary structure and grain size distribution was done by reflected light- and scanning electron microscopy (SEM). Polished and etched thick sections of the annealed samples were produced by using the method described in Urai et al. (1987). The sample's surface was carefully ground and polished. Then the section was immersed and agitated in slightly undersaturated NaCl solution (~5.5 molar) for 10 seconds. The solution was removed by rinsing the section with a powerful jet of cyclohexane. It was quickly dried with a hot air blower and stored under dry conditions.

Fractured surfaces

For observation of grain surfaces by SEM the samples were broken in tension directly after removal from the annealing cell and stored under dry conditions.

Grain size measurements

Grain size was measured at different stages of annealing. The size of large grains formed by *primary recrystallization* and *exaggerated grain growth* (see below) was measured only on grains that were rectangular in the section plane (sectioned normal to opposite cube faces), whereas the grain size during *normal grain growth* was measured using the intercept method (Underwood 1970).

Results

An overview of the samples described in this paper is given in Table 1.

Water content

The water content of the samples was calculated from the weight loss due to evaporation by drying. The brine-filled, connected porosity is $2.5 \pm 0.5\%$ for both fine- and coarse-grained samples.

In addition the water content was measured for one annealed, fine-grained sample by infrared spectroscopy (A. Kronenberg, pers. communication) which indicated ~660 ppm H_2O. The discrepancy with the higher values found by drying can be explained by the failure of infrared spectroscopy to detect fluid-filled pores much larger than 1 μm, as these are going to absorb the IR photons at the OH band wave number extremely effectively (Kronenberg, pers. communication).

Comparison with dry samples

It is generally accepted that completely water-free samples of NaCl do not recrystallize at room temperature. Franssen (1993) and Guillopé and Poirier (1979) have shown that dry grain boundaries become mobile at temperatures above 450 °C. To validate this for our samples, we examined the nominally dry samples with cyclohexane as pore fluid. Reflected light microscopy of these samples shows an almost total absence of recrystallization, with a few local occurrences of small new grains. We interpret these to be the consequence of small fluid inclusions in the grains, which were not fully removed by the drying procedure. Another method to dry the NaCl is to melt it, and grind the solidified mass into

Table 1 Overview of samples described in this paper

Sample	Type of salt	Starting grain size (μm)	Annealing time (d)	Storage[a]
OS-003c	Table salt	> 355	2.79	S
OS-003d	Table salt	> 355	4.97	S
OS-023c	Roth	< 50	98.18	S
OS-039a	Roth	< 50	0.04	N
OS-039b	Roth	< 50	0.09	N
OS-041a	Roth	< 50	5.83	N
OS-048	Roth	< 50	-	O
OS-063c	Roth	< 10	3.99	N
OS-063d	Roth	< 10	33.15	N
OS-065a	Roth	< 10	0.17	N
OS-065b	Roth	< 10	0.90	N
OS-065c	Roth	< 10	7.05	N
OS-065d	Roth	< 10	29.02	N
OS-070a	Roth	< 10	0.01	N
OS-070b	Roth	< 10	0.17	N
OS-070c	Roth	< 10	20.20	N
OS-071a	Roth	< 10	0.80	N
OS-071b	Roth	< 10	4.78	N
OS-072a	Roth	< 10	0.02	N
OS-072b	Roth	< 10	0.05	N
OS-073a	Roth	< 10	0.07	N
OS-073b	Roth	< 10	0.08	N
OS-074a	Roth	< 10	0.11	N
OS-074b	Roth	< 10	0.13	N
OS-075a	Roth	< 10	19.00	N
OS-075b	Roth	< 10	27.00	N
OS-085a	Roth	200–355	0.02	N
OS-085b	Roth	200–355	0.23	N
OS-086a	Roth	200–355	1.05	N
OS-086b	Roth	200–355	1.34	N
OS-088a	Roth	200–355	4.08	N
OS-088b	Roth	200–355	6.06	N
OS-089a	Roth	200–355	7.98	N
OS-090a	Roth	200–355	32.08	N
OS-090b	Roth	200–355	39.10	N
OS-091b	Roth	200–355	48.24	N
OS-092a	Roth	200–355	59.36	N
OS-093a	Roth	200–355	53.05	N
OS-096a	Roth	200–355	2.15	N
OS-097a	Roth	200–355	2.21	N
OS-111a	Roth	< 10	1.17	N
OS-111b	Roth	< 10	4.13	N
OS-114a	Roth	< 10	11.05	N
OS-117a	Roth	< 10	0.67	N
OS-118	Roth	< 10	-	O
OS-119a	Roth	< 10	0.01	N
OS-120a	Roth	< 10	0.56	N
OS-121	Roth	< 50	-	O
OS-122	Roth	< 50	-	O
OS-123	Table salt	> 355	-	O
OS-124	Table salt	> 355	-	O

[a]S, stored in air with silica gel; N, stored in air with humidity buffered by saturated NaCl solution; O, dried at 104 °C for 3 days

a fine powder. Samples prepared by this method, and pressed dry into dense blocks show the total absence of recrystallization (JLU, unpublished observations).

Microstructural evolution of coarse-grained samples (''primary recrystallization'')

The deformation of the initial cube-shaped grains was clearly shown by the irregular grain shapes, the abundant defect structure and by microcracks initiated at grain boundaries (Fig. 3a). Nucleated in these high-strain zones, new grains start to grow after a few

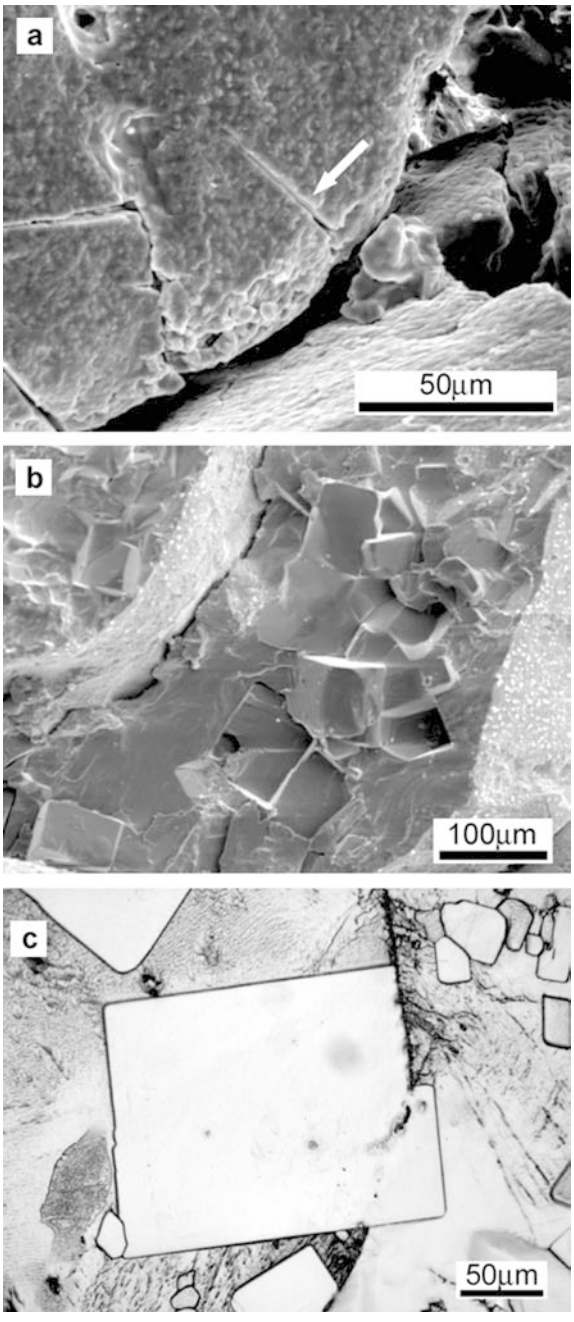

Fig. 3a–c Micrographs of coarse-grained samples. See Table 1 for a detailed description of the respective samples (also relevant to all sample micrographs shown in this paper). **a** SEM image of a broken surface of sample OS-003d showing microcracks (see *arrow*) and other damage on grain surfaces pointing to locally high defect density favorable for nucleation of primary recrystallization. **b** SEM image of a broken surface of sample OS-003c illustrating primary recrystallized grains. Note the difference of the surface morphology of old and new grains. **c** Reflected light image of a polished and etched surface of sample OS-012c showing the growth of euhedral new grains during primary recrystallization. Boundaries between two new grains do not show evidence of mobility. Note the abundant defect structure in the deformed old grains

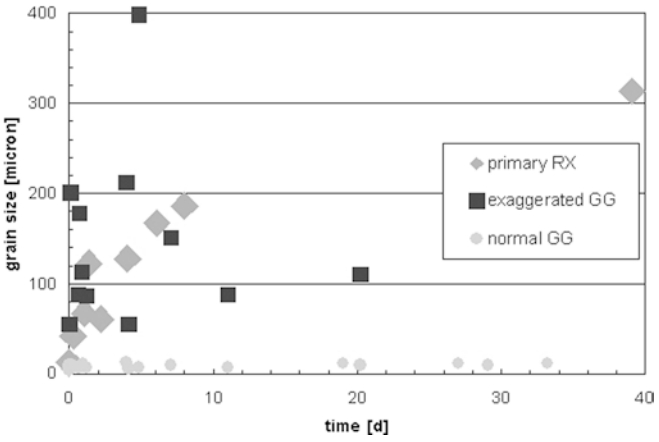

Fig. 4 Combined diagram of grain size versus annealing time data for the three different types of grain boundary migration described in this paper (see text for methods of measurements and Table 1 for further details). Note the decrease in growth rate during primary recrystallization, the large scatter of data in secondary recrystallization (exaggerated grain growth) and the essentially zero growth rate in normal grain growth

hours of annealing (Fig. 3b, c). These grains continue to grow into the surrounding deformed grains until they meet another recrystallized grain. Usually new grains are pinned at old grain boundaries, but sometimes they grow across old grain boundaries (Fig. 3c). Most new grains tend to be euhedral, but often the grain edges are not sharp, and curved grain boundaries also occur.

Figure 4 shows the size of these euhedral grains fully enclosed within deformed old grains, as a function of annealing time. Initially grain boundary migration rates are of the order of 2–6 nm/s, but with increasing time of annealing the growth rate decreases. Although the grains are euhedral, it is noted that the grains' corners are in fact not sharp (Figs. 3c and 5). SEM observations show that these rounded corners consist of smaller facets, which have generally the same orientation as the large faces. However, also facets with orientations other than {100} were found (Fig. 5).

In cross section, indications of fluids in the boundaries of these primary recrystallized grains are efflorescence (Fig. 5) and grain boundary voids with a thickness of less than 100 nm. Most commonly however, a separation between the two grains (which could have contained a fluid film) could not be resolved at the limits of resolution of the SEM. In plane view, some details of the internal structure of the grain boundaries could be resolved, showing a regular network of slight depressions on the surface of the grain being consumed (Fig. 6).

The occurrence of efflorescence on both polished and broken surfaces was commonly patchy, with some parts showing strong efflorescence and others none at all. This observation also holds for the fine-grained samples, and its significance will be discussed further below.

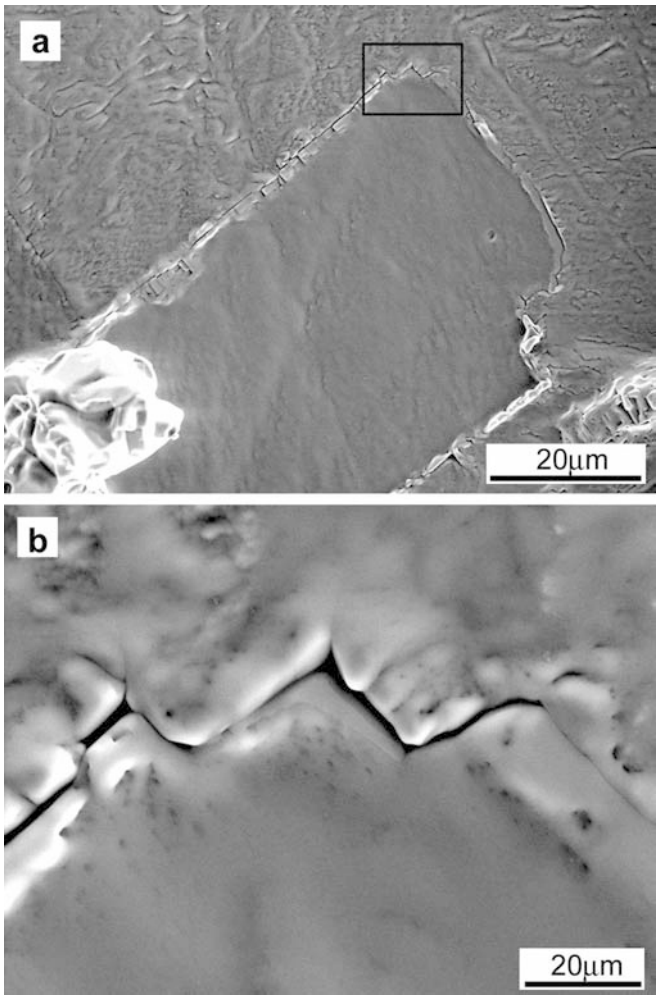

Fig. 5a,b SEM micrographs of a polished and etched surface of sample OS-092a showing the euhedral growth of primary recrystallizing grains by consuming deformed material. The trace of the grain boundary is covered by efflorescence. The detail (**b**) illustrates the shape of the 'rounded' corners, with 'stepped' growth according to the crystallographic system. Efflorescence at the boundary of the recrystallized grain points to existence of fluids

Microstructural evolution of fine-grained samples

''Recrystallization and grain growth''

Compaction of the wet, fine-grained slurry also produces dense aggregates. The grain size versus time data is shown in Fig. 4. It can be seen that even for long annealing times there is no significant grain growth. Closer observation of the microstructure during the first hours of annealing does reveal a reduction of grains with a visible internal defect structure, a reduction of irregularities in grain boundaries, and some rearrangement of porosity (Fig. 7).

Using the grain size versus time data from primary recrystallization (Fig. 4), we estimate the time required to completely replace deformed grains by primary recrystallization in these fine-grained samples to be less

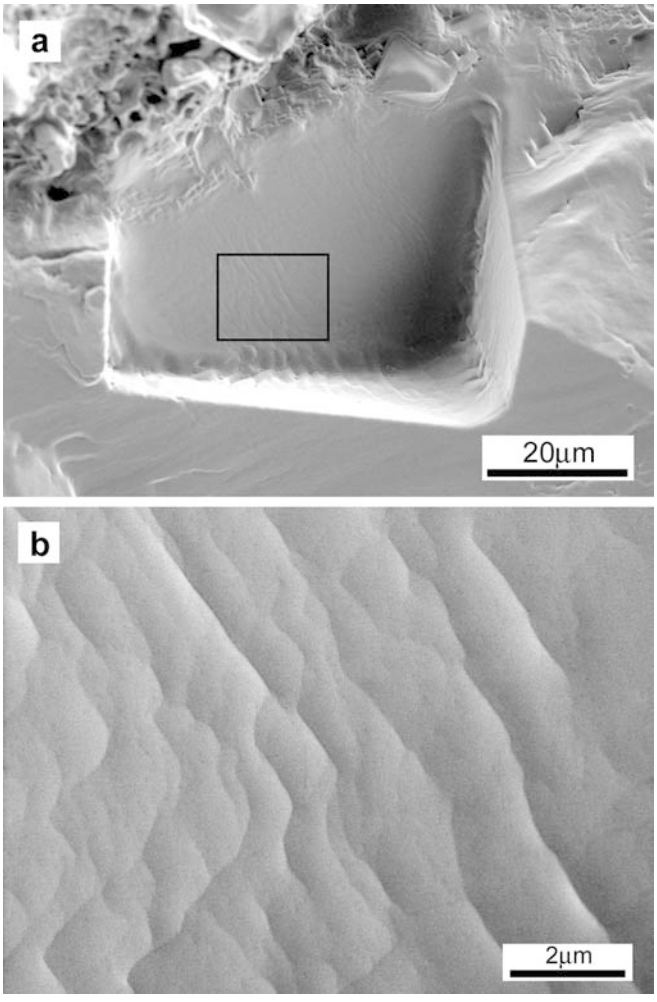

Fig. 6a,b SEM micrographs of a broken surface of sample OS-097a showing a negative imprint of a recrystallized grain. Note the structured interface of the old grain: the *parallel bands* (shown in the detail **b**) are interpreted as etch pit-like structures related to dislocation networks inside the old grain (see also sketch in Fig. 12a)

than 5 hours. Therefore we infer that primary recrystallization is largely completed after this period, in agreement with our observations (Fig. 8).

Efflorescence in large parts of the sample surface always formed during preparation of the fine-grained samples (Fig. 9), regardless the time of annealing. If the samples are oven-dried before polishing and etching, the surface structure is similar, but no efflorescence is formed. However, there were always parts of the surface that formed no efflorescence. These locations were usually small protrusions on the broken surface (Fig. 9a).

These areas without efflorescence allow observation of the grain boundary structure in broken samples. The main feature is the occurrence of angular grains with planar boundaries. Porosity is located predominantly at triple junctions, and sometimes between grains. The planar parts of the grain boundaries are smooth, showing only a few irregularities resolvable at the resolution of SEM, but with a clearly defined rim, connected with the triple junction porosity. This observation is equivalent to the clearly defined dihedral angles observed in images showing boundaries in profile. Dihedral angles are highly variable: they range between ~20 and 110°, associated with the tendency of many grains to develop rectangular shapes (Fig. 10).

"Exaggerated grain growth"

In most fine-grained samples exaggerated grain growth was observed. These grains are much larger than the starting grain size of 10 µm and consume the surrounding fine grains. They are characterized by their rectangular shape (Fig. 11). As shown in Fig. 4 the size of these grains increases with time of annealing but with a decreasing growth rate, similar to primary recrystallized grains. These grains mostly appear in a fine-grained matrix (Fig. 11). They are predominantly free of inclu-

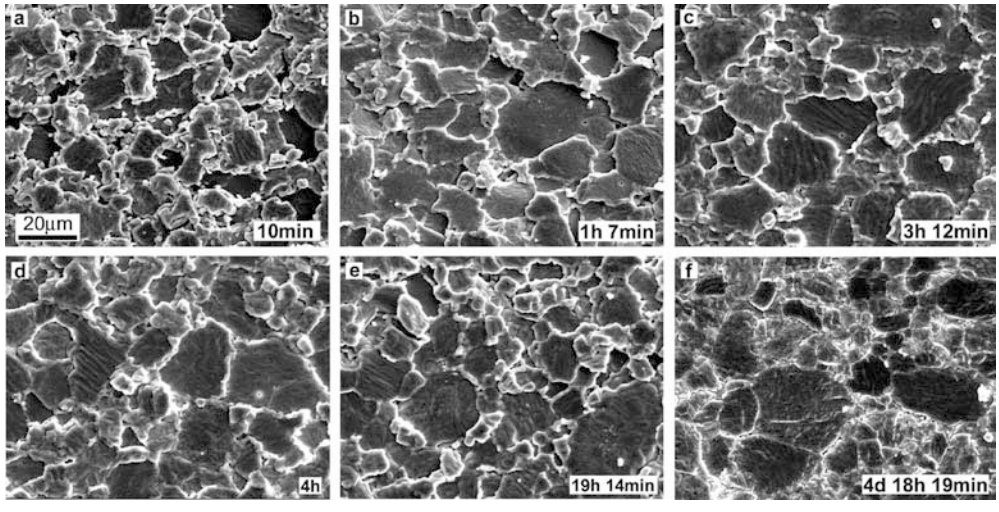

Fig. 7a–f Series of SEM micrographs of polished and etched surfaces of the samples: **a** OS-070a; **b** OS-072b; **c** OS-074b; **d** OS-070b; **e** OS-071a and; **f** OS-071b illustrating the evolution of grain structure with time. With increasing time the serrated grain boundaries straighten out and the defect structure in the grains is reduced. After one hour of annealing a further increase in grain size ceases

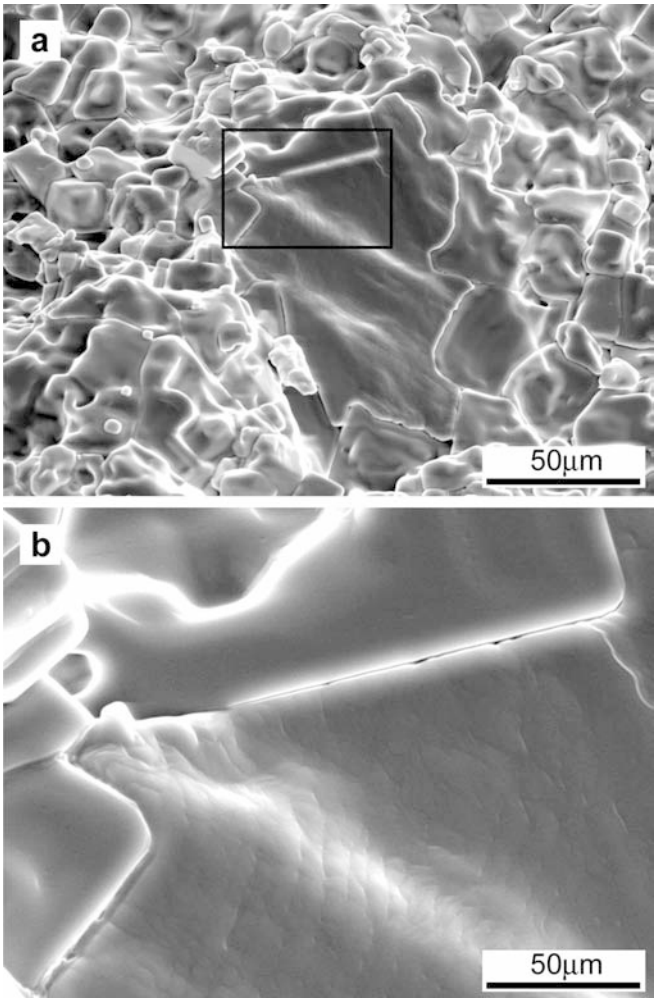

Fig. 8 **a** SEM micrograph of a broken surface of sample OS-039b illustrating primary recrystallization during the first hours of annealing of the fine-grained samples. The large grain in the central part of the image is a deformed old grain being consumed by a defect-free grain with generally low index faces, but also faces different from {100} are found at the recrystallized grain's corner (**b**). **b** *Inset* shown in **a**

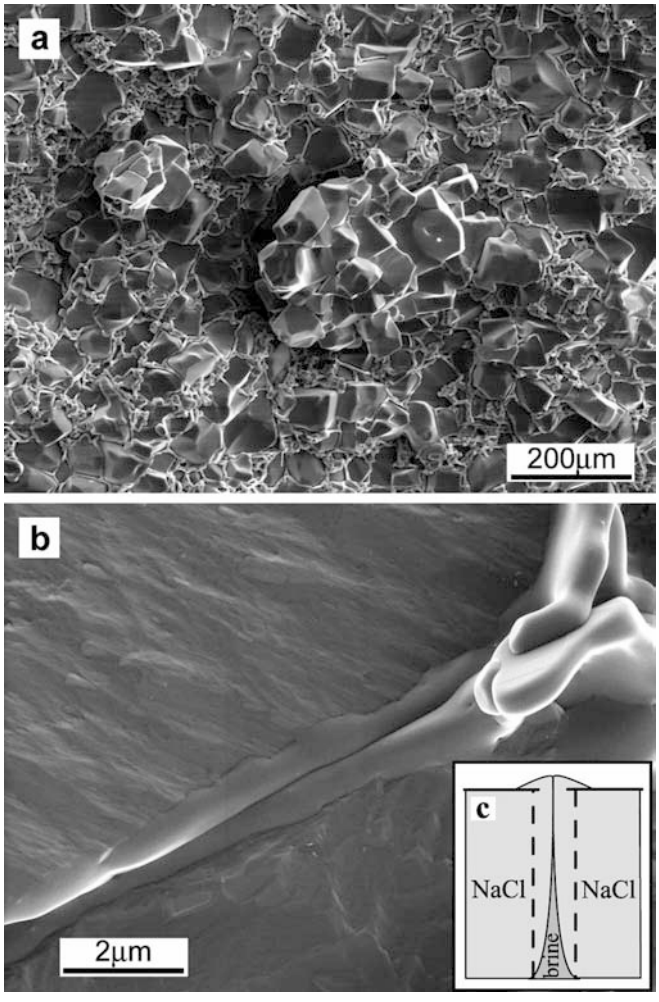

Fig. 9 **a** Sample OS-041a; **b** Sample OS-114a. SEM micrographs of samples OS-041a (broken surface) and OS-114a (polished and etched surface) showing the effects of efflorescence. In **a**, the central part develops no efflorescence: we infer that it is isolated from the fluid-filled network in the sample, whereas **b** shows the efflorescence in detail. *Inset* **c** is a sketch illustrating the capillary-driven transport of brine that leads to efflorescence resulting in deposition of larger amounts of halite around grain boundaries emerging at the sample surface

sions, but rarely cigar-shaped inclusions are found inside them.

At low magnification the boundaries of these new grains appear straight, but high magnification micrographs show that they are irregular at length scales of the small matrix grains (Fig. 11). The grain boundary separating the large new grains from the matrix is commonly free of pores visible at the resolution of SEM.

Discussion

In agreement with much previous work, these experiments show that the presence of small amounts of brine has a major effect on grain boundary migration in sodium chloride. This effect is absent in samples containing a non-polar fluid.

The wet samples have a fluid-filled porosity of $2.5 \pm 0.5\%$ and very few gas bubbles which were carefully avoided by the preparation procedure. Many pores are relatively large and form a connected network, in agreement with microstructural observations and the drying data.

The sample preparation process exposed the pore fluid in the samples to dry air. As shown by the efflorescence, this resulted in migration of the fluid and crystallization from the evaporating brine. This effect was surprising, because the results of Lewis and Holness (1996) report at conditions of 1 bar and 25 °C contact angles at which porosity should not be connected.

Evaporation of immobile brine from a pore produces a coherently grown sodium chloride layer with a thickness of 16% of the brine's volume. Evaporation in combination with capillary forces and a mobile and

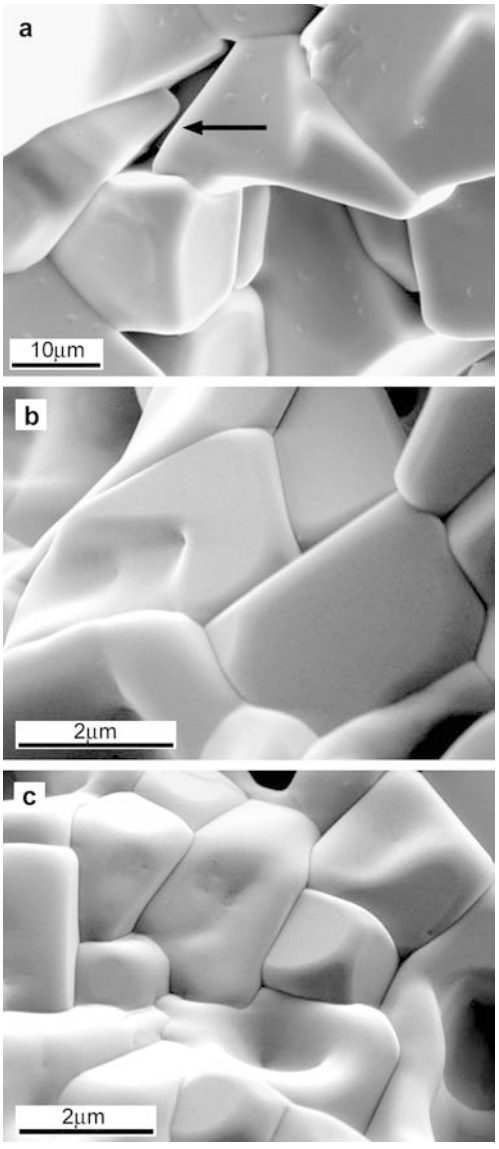

Fig. 10 **a** Sample OS-041a; **b**, **c** Sample OS-114a. SEM micrographs of efflorescence-free broken surfaces of samples **a**, OS-041a and **b**, **c** OS-114a illustrating grains with their characteristic smooth planar surfaces, with sometimes minor elevations at the grains' edges. These structures indicate contact healing. The porosity is predominantly in triple junction channels. In these figures the grains are thought to have completely healed grain boundaries and grain growth is stopped. Note the tendency of the grains to develop rectangular shapes and also note the broad range of contact angles in **a** (see *arrow*; *small bumps* in this section are artifacts)

connected fluid phase will have a larger effect: the fluid locally drains towards the surface, where it evaporates, producing the observed efflorescence structures (see Fig. 9). In these locations this may strongly obscure the original grain boundary structure. On the other hand, this flow of the brine will also effectively drain the pore fluid from some other areas of the sample surface. This drainage of brine away from the external surface is interpreted to be the reason for efflorescence-free regions, which can be used to study the details of the grain

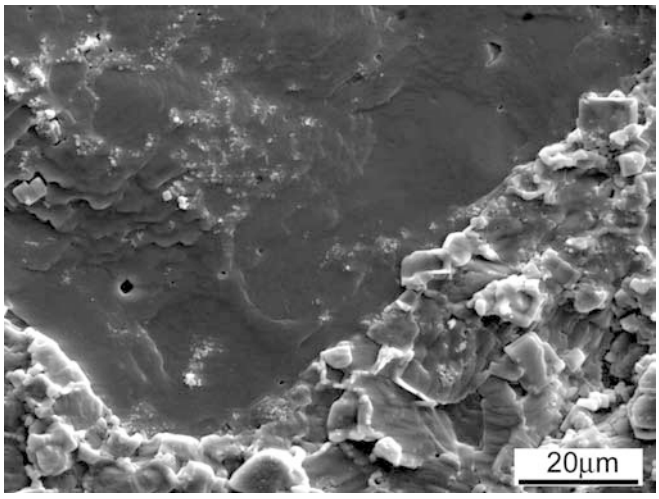

Fig. 11 SEM micrograph of a polished and etched surface of sample OS-117a showing the grain boundary of an exaggerated grain characterized by predominantly straight grain boundaries. Along these boundaries it consumes the fine-sized grains of the matrix

boundaries (compare Fig. 9a). Therefore we interpret the efflorescence-free parts of the microstructure to represent the in-situ structure with the brine removed, with only minor modification due to sample preparation.

Primary Recrystallization

Euhedral primary recrystallized grains are also observed by Skrotzki and Welch (1983) from extrusion experiments at room temperature, pointing to brine on the grain boundary probably derived from fluid inclusions inside the deformed matrix. In experiments and in nature, however, curved and euhedral grains are both common.

In agreement with extensive literature, we interpret the results of the coarse-grained samples as follows.

The pressing of the coarse-grained, cube-shaped powders caused deformation of the grains, which is shown by their deformed shape and internal defect microstructure containing dislocation networks and microcracks. Annealing at room temperature does not allow recovery processes inside the deformed grains. The compaction-caused defect density is highest in the old grain boundary regions, leading to nucleation of strain-free grains at these sites (Humphreys and Hatherly 1996). We note that differences in dislocation density are expected inside the old grains, and thus driving forces for grain boundary migration will vary. This is in agreement with the scatter in initial growth rates of the new grains. Primary recrystallization then proceeds in an isotropic stress field of 1 atmosphere.

The structure of the migrating boundaries could not be observed in detail using the techniques of this study. Arguments in favor of the interpretation of the existence

of fluid-enriched zones on grain boundaries are (1) the frequent efflorescence from such boundaries, (2) the euhedral shape of the growing grains, and (3) the high migration rates. In agreement with previous work, we interpret the boundaries to continue a semi-continuous water-enriched zone with a thickness less than about 50 nm. If the zone were thicker, we would have resolved a separation between the grains in the SEM. It was somewhat surprising to find so little evidence of thicker migrating fluid films in these samples, as a normal stress is absent and there is no a priori reason for initially thicker boundary films to start migrating.

Normal grain growth

The presence of fluids also plays a major role for the fine-grained samples as it enhances the mobility of the grain boundaries for primary recrystallization of the deformed grains. In agreement with the rates observed in coarse-grained samples, primary recrystallization is interpreted to be similar to that in the coarse-grained samples, but come to completion much more rapidly. Both broken and polished and etched SEM micrographs show the rearrangement of grains, grain boundaries and porosity being completed after several hours.

After this time, the grain growth essentially stops. Considerations of the driving force for grain growth suggest that this is not just a much slower process, which might be significant at even longer time scales (Fig. 4). We interpret the grain size versus time data, in combination with the clear contact angles as an indication of a fundamental change in grain boundary mobility: at conditions of 1 bar and 25 °C neck growth is initiated and the mobile grain boundaries reorganize into fluid-free boundaries connecting the network of brine channels in the triple junction network. This essentially stops grain growth. Under a small external stress field a similar process was observed by Visser (1999) in fine-grained sodium nitrate.

A final point worth considering is why in our fine-grained samples neck growth in grain boundaries does not lead to the formation of arrays of fluid inclusions. This can be explained by the commonly reported characteristic size of such inclusions in coarse-grained halite (Urai et al. 1986b). This size is almost as large as the grain size in our samples, so that almost without exception neck growth leads to redistribution of the fluid into the triple junction network.

The morphologies of grain edges and triple junctions with a broad range of contact angles (20 to 110°) are interpreted to be caused by the high surface anisotropy of the initial wet grain boundaries. This leads to a change in the morphologies around the triple junctions, and local large deviations from the theoretical contact angle based on isotropic surface energies. This results in a mosaic of small-sized grains with straightened grain boundaries and with a broad spectrum of contact angles (Fig. 10). Efflorescence still found in samples after annealing for months is evidence for fluid mobility through this network, in agreement with the wide range of contact angles. This is in contrast to the observations found by Lewis and Holness (1996) who argued that at similar conditions (1 bar and ~25 °C) the contact angles are about 70° resulting in non-permeability of salt rocks.

Exaggerated grain growth

Because of its similarity to primary recrystallization, exaggerated (abnormal or discontinuous) grain growth is also called secondary recrystallization. This process requires an already recrystallized structure, in which grain growth is impeded, unless some grains enjoy some advantages other than size over its neighbors (Humphreys and Hatherly 1996). According to these authors such advantages are second phase particles, texture and surface effects. As for normal grain growth, this process is driven by the reduction in grain boundary energy resulting in grain boundary area reduction during coarsening (Detert 1978; Evans et al. 2001).

As for the coarse-grained samples, exaggerated grain growth takes place under static conditions. Its driving force is the stored energy inside the volume of fine-grained matrix that is being consumed.

Secondary recrystallization starts after normal grain growth already stopped. The fine-grained matrix consists of grains all with different orientation resulting in surface energy variations between the grains (Humphreys and Hatherly 1996). As the surface energy of a grain itself is strongly dependent on the surface chemistry, fluids existing on grain boundaries and in triple junction tubes have also a major effect on the onset of secondary recrystallization. We interpret the observations as follows: the abnormal growing grain consumes the neighboring fine-grained matrix and the grain boundary fluid-rich zone incorporates fluids present in pores. As for primary recrystallization the fluids are assumed to be distributed uniformly on the mobile grain boundaries, so that the grain continues its growth into a euhedral shape indicating again the fluid-dependent anisotropy of surface energies. In ceramics similar processes are well known: exaggerated grain growth with large faceted grains are explained by anisotropy of surface energies (Kingery 1974).

Nature of grain boundary fluid

Although direct observation of the fluid in mobile grain boundaries was not possible in this study, all our observations led us to the interpretation of their presence. If the fluid-enriched zone has short-range thickness variations, these should be commonly less than 50 nm. Below this length scale the thickness of the fluid is not resolved.

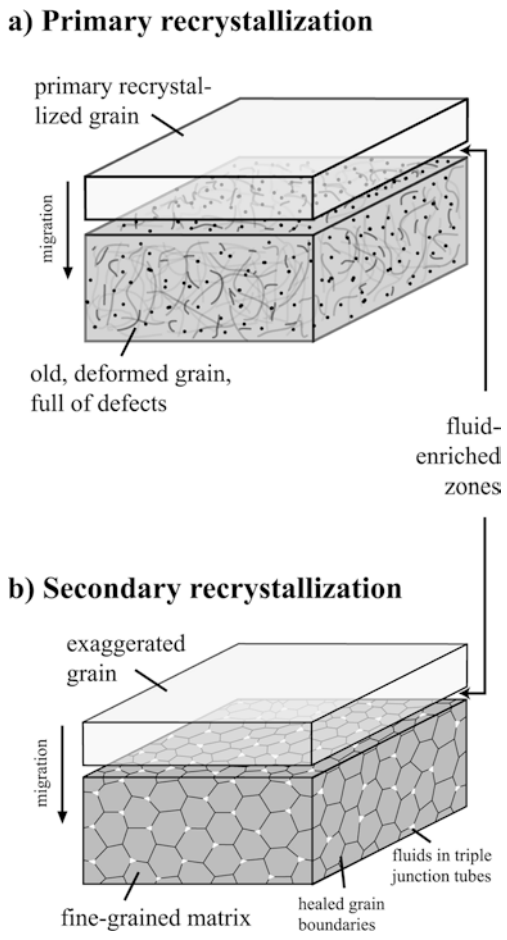

Fig. 12a,b Schematic illustration of the hypothesis of the structure of migrating brine-filled grain boundaries. **a** Primary recrystallization: the strain-free grain consumes the deformed grain indicated by dislocations. Dissolution is interpreted to be favored at etch pit-like structured locations. **b** Secondary recrystallization: the exaggerated grain consumes the fine-grained matrix by incorporating the fluids that are residing in a network of triple junction tubes. Similar to **a**, these areas are preferred dissolution sites. For both processes, the thickness of the fluid-enriched zones is assumed to be less than 50 nm

There is however a clear difference in lateral structure of grain boundaries in primary recrystallization and exaggerated grain growth, illustrated in Fig. 12.

In primary recrystallization the new grain is growing into an old one with a high dislocation density. Our observations suggest that the primary morphological factor on the surface of the grain being dissolved is the array of etch pits around the termination of dislocation arrays on the grain surface. At these sites the rate of dissolution is slightly higher, and in combination with the euhedral new grains this is proposed to lead to a thickness variation of the grain boundary fluid-rich zone.

In exaggerated grain growth the migrating grain boundaries are permanently connected to the terminations of fluid-filled triple junction tubes (Fig. 12b). In between these, there are the dry grain boundaries, which are being consumed. We propose that an etch-pit like structure is also present here, forming a system of fine channels in the grain boundary, which are connecting the triple junction tube terminations. One possible explanation for the observation that exaggerated-grown grains are free of inclusions is that the fluid that might be otherwise collected in the moving grain boundary is removed from the system by flow along the triple junction tubes.

To get more information on the properties such as thickness and morphology of these brine-filled grain boundaries we are starting direct observations in a cryogenic SEM, in which the fluids will be frozen before breaking the sample.

Acknowledgements We are grateful to Andreas Kronenberg for carrying out the infrared spectrometry. Uwe Wollenberg and Jörg Kallinna provided essential assistance with SEM. The manuscript was significantly improved by two anonymous reviewers. This project was funded by the Deutsche Forschungsgemeinschaft (UR 64/4–1).

References

de Bresser JHP, Ter Heege JH, Spiers CJ (2001) Grain size reduction by dynamic recrystallization: can it result in major rheological weakening? Int J Earth Sci (Geologische Rundschau) 90:28–45

de Meer S, Spiers CJ, Peach CJ, Watanabe T (2002) Diffusive properties of fluid-filled grain boundaries measure delectrically during active pressure solution. Earth Planet Sci Lett 200:147–157

Detert K (1978) Secondary recrystallization. In: Haessner F (ed) Recrystallization of metallic materials. Dr. Riederer Verlag GmbH, Stuttgart, pp 97–109

Drury MR, Urai JL (1990) Deformation-related recrystallization processes. Tectonophysics 172:235–253

Evans B, Renner J, Hirth G (2001) A few remarks on the kinetics of static grain growth in rocks. Int J Earth Sci (Geologische Rundschau) 90:88–103

Fokker PA, Urai JL, Steeneken PV (1996) Production-induced convergence of solution mined caverns in magnesium salts and associated subsidence. In: Proc Int Conf Land Subsidence, Den Haag, pp 281–289

Franssen RCMW (1993) Rheology of synthetic rocksalt with emphasis on the influence of deformation history and geometry on the flow behaviour. Universiteit Utrecht, Geologica Ultraiectina 113, 221 pp

Garcia Celma A, Urai JL, Spiers CJ (1988) A laboratory investigation into the interaction of recrystallization and radiation damage effects in polycrystalline salt rocks. Nuclear Science and Technology, CD-NA 11849EN

Guillopé M, Poirier JP (1979) Dynamic recrystallization during creep of single-crystalline halite: an experimental study. J Geophys Res 84:5557–5567

Hickman SH, Evans B (1991) Experimental pressure solution in halite; the effect of grain/interphase boundary structure. J Geol Soc Lond 148:549–560

Hilgers C, Koehn D, Bons PD, Urai JL (2001) Development of crystal morphology during unitaxial growth in a progressively widening vein; II, Numerical simulations of the evolution of antitaxial fibrous veins. J Struct Geol 23:873–885

Hilgers C, Urai JL (2002) Microstructural observations on natural syntectonic fibrous veins: implications for the growth process. Tectonophysics 352:257–274

Holness M, Lewis S (1997) The structure of the halite-brine interface inferred from pressure and temperature variations of equilibrium dihedral angles in the halite-H_2O-CO_2 system. Geochim Cosmochim Ac 61:795–804

Humphreys FJ, Hatherly M (1996) Recrystallization and related annealing phenomena. Pergamon Press, Oxford, 497 pp

Jackson MPA, Talbot CJ (1986) External shapes, strain rates, and dynamics of salt structures. Geol Soc Am Bull 97:305–323

Kingery WD (1974) Plausible concepts necessary and sufficient for interpretation of ceramic grain-boundary phenomena: II, Solute segregation, grain-boundary diffusion, and general discussion. J Am Ceramic Soc 57:74–83

Lewis S, Holness M (1996) Equilibrium halite-H_2O dihedral angles: high rock-salt permeability in the shallow crust? Geology 24:431–434

Martin B, Roeller K, Stoeckhert B (1999) Low-stress pressure solution experiments on halite single-crystals. Tectonophysics 308:299–310

Miralles L, Sans M, Gali S, Santanach P (2001) 3-D rock salt fabrics in a shear zone (Suria anticline, South-Pyrenees). J Struct Geol 23:675–691

Peach CJ (1991) Influence of deformation on the fluid transport properties of salt rocks. Universiteit Utrecht, Geologica Ultraiectina 77, 238 pp

Peach CJ, Spiers CJ, Trimby PW (2001) Effect of confining pressure on dilatation, recrystallization, and flow of rock salt at 150 °C. J Geophys Res 106:13,315–13,328

Schutjens P (1991) Intergranular pressure solution in halite aggregates and quartz sands: an experimental investigation. Universiteit Utrecht, Geologica Ultraiectina 76, 233 pp

Skrotzki W, Welch P (1983) Development of texture and microstructure in extruded ionic polycrystalline aggregates. Tectonophysics 99:47–61

Smith CS (1964) Some elementary principles of polycrystalline microstructure. Metall Rev 9:1–48

Spiers CJ, Brzesowsky RH (1993) Densification behaviour of wet granular salt: theory versus experiment. In: 7th Symposium on Salt. Elsevier Science, Amsterdam, pp 83–92

Spiers CJ, Schutjens P (1990) Densification of crystalline aggregates by fluid-phase diffusional creep. In: Meredith PD (ed) Deformation processes in minerals, ceramics and rocks. Unwin Hyman, London, pp 334–353

Spiers CJ, Schutjens PMTM, Brzesowsky RH, Peach CJ, Liezenberg JL, Zwart HJ (1990) Experimental determination of constitutive parameters governing creep of rocksalt by pressure solution. In: Rutter EH (ed) Deformation mechanisms, rheology and tectonics. Geological Society Special Publication 54, pp 215–227

Talbot CJ, Rogers EA (1980) Seasonal movements in a salt glacier in Iran. Science 208:395–396

Underwood EE (1970) Quantitative stereology. Addison-Wesley Publishing Company, Reading, MA, 274 pp

Urai JL, Means WD, Lister GS (1986a) Dynamic recrystallization of minerals. In: Heard HC (ed) Mineral and rock deformation; laboratory studies; the Paterson volume. AGU Geophysical Monograph, pp 161–199

Urai JL, Spiers CJ, Zwart HJ, Lister GS (1986b) Weakening of rock salt by water during long-term creep. Nature 324:554–557

Urai JL, Spiers CJ, Peach C, Franssen RCMW, Liezenberg JL (1987) Deformation mechanisms operating in naturally deformed halite rocks as deduced from microstructural investigations. Geologie en Mijnbouw 66:165–176

Visser HJM (1999) Mass transfer processes in crystalline aggregates containing a fluid phase. Universiteit Utrecht, Geologica Ultraiectina 174, 244 pp

Watanabe T, Peach CJ (2002) Electrical impedance measurement of plastically deforming halite rocks at 125 °C and 50 MPa. J Geophys Res 107:1–12

Wenkert DD (1979) The flow of salt glaciers. Geophys Res Lett 6:523–525